RSC Advances

RSC Publishing

PAPER

Simultaneous positioning and orientation of single nano-wires using flow control†

Cite this: *RSC Advances*, 2013, **3**, 2677

Pramod P. Mathai,*[ab] Peter T. Carmichael,[a] Benjamin A. Shapiro[acd] and J. Alexander Liddle[a]

Received 5th December 2012,
Accepted 11th December 2012

DOI: 10.1039/c2ra23190e

www.rsc.org/advances

We present a material-property independent method for manipulating both the position and orientation of nanowires (NWs), by feedback control of flows. For example, the NWs need not be electromagnetically polarizable. Control of NWs in a microfluidic device is demonstrated across a 170 μm × 170 μm region with on-demand trapping, translation, and simultaneous rotation of dielectric, semiconducting, and metallic NWs. An average trapping precision of 0.6 μm in position and 5.4° in orientation is achieved for the NWs considered, making it attractive for sensing and directed assembly applications.

1 Introduction

Sensing and directed assembly applications that use single nanoscale objects require control over their position and orientation. The ability to position and orient individual NWs can be used to build structures that sense and guide electromagnetic waves,[1,2] steer a nanowire (NW) light source to image nanostructures,[3] manipulate NWs to precisely deliver chemical doses to specific parts of a cell,[4] and align NWs to detect chemicals[5] by monitoring structural changes along the alignment direction caused by chemical adsorption. Such an ability could also be used to map intensities and polarizations of microscale force fields over a large area using nanowire probes. Flow control has the advantage that the controlled fluid can exert forces and hence manipulate objects of any material type. Since viscous forces scale with object length rather than volume, electro-osmotic flow control (EOFC) has enabled the positional manipulation of nanoscopic objects that are difficult to actuate by optical and dielectrophoretic means, and has done so with nanoscale precision.[6]

Prior techniques for manipulating both the position and orientation of nanoscale objects include sculpting optical wavefronts to rotate optically polarizable objects[7–14] or using plane wavefronts to rotate birefringent ones,[15,16] using dielectrophoretic forces to position and orient objects that are polarizable at radio frequencies,[17–25] and magnetic actuation to manipulate magnetically susceptible objects.[26–29] A common feature of all these techniques is that they rely on intrinsic material properties, such as polarizability, of the manipulated object[7–29] (or of those in its vicinity[30]). A magnetic field for example, cannot directly control a non-magnetic object.

Here we show how precise flow control using EOF can be used to control not only the position, but also simultaneously the orientation, of NWs in a 2D plane. Instead of using forces and torques that rely on the properties of the wire, we create electro-osmotically actuated flow patterns that move and rotate the wire by viscous stresses. We achieve essentially the same degree of control over dielectric, semi-conducting and conducting NWs, thus showing that the technique is effective regardless of the material properties of the nano-object. The NWs are controlled in a simple polydimethyl siloxane (PDMS)-mold-based device, with a one-time requirement for mold microfabrication.

2 Results and discussion

An electric field applied across a microfluidic channel creates a plug flow (EOF) whose velocity is directly proportional to the field strength[31,32] (see ESI† for details on EOF physics). An immersed nano-object moves with the local flow velocity due to the applied viscous stress, which depends on the object's dimensions and orientation.

Here we use EOF within a vision-based feedback loop to control the NW motion as shown in Fig. 1. Since electric fields are curl-free one cannot create a circulating flow to rotate the object. Instead, shear flows are used to rotate objects with less symmetry than a sphere, *e.g.* a NW,[33] as shown in the top

[a]*Center for Nanoscale Science and Technology (CNST), National Institute of Standards and Technology (NIST), 100 Bureau Drive, Gaithersburg, MD, USA. E-mail: ppm@umd.edu*
[b]*Maryland Nanocenter, Kim Engineering Building, University of Maryland (UMD), College Park, MD, USA*
[c]*Fischell Department of Bioengineering, UMD, College Park, MD, USA*
[d]*The Institute for Systems Research, UMD, College Park, MD, USA*

† Electronic Supplementary information (ESI): Supplementary text and movies can be downloaded. Movie M1 (sped up to 4× real time) shows control of the SU8 rod along the ''NIST'' path. Movies M2, M3 and M4 (all real time) shows rotation and trapping of SU8, silicon and gold NWs respectively. DOI: 10.1039/c2ra23190e

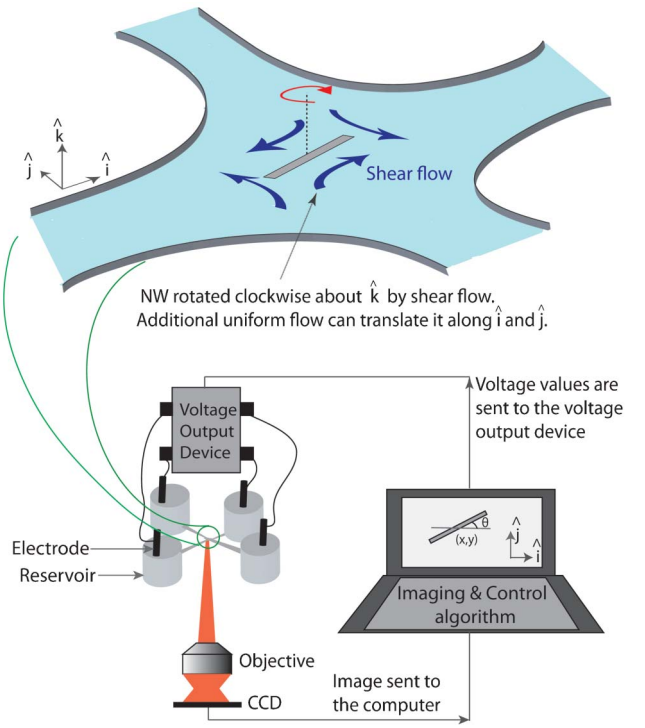

Fig. 1 Schematic of the microfluidic device (top, magnified) and the feedback hardware loop (bottom). The position and orientation of the NW (grey rod) is observed through the microscope objective at each time step. Based on this, a computer algorithm determines the quartet of voltages that will create a fluid flow (blue arrows) to translate and rotate the NW from where it is towards where it should be (only rotation is shown in the figure). The same process repeats at the next time step to continuously move and rotate the NW along its desired trajectory.

panel of Fig. 1. Voltages applied at peripheral electrodes create EOF in the four microchannels and in the central control region where the four channels meet. Precise NW manipulation, using controlled translational and shear flows, is achieved by choosing the strength and orientation of the electric field guiding the EOF based on the NW's current position and orientation.

Each cycle of the feedback loop starts with the charge-coupled device (CCD) camera sensing the NW image. An image processing algorithm estimates the NW's position and orientation using centroiding and least-squared best-fits respectively (see ESI for details of position and orientation estimation†). These estimates are compared to the next targeted position and orientation along a user-specified trajectory. The difference is multiplied with constant gain parameters—one for position and one for orientation—giving the needed translational and rotational velocity of the NW that will take it to the next desired target position and orientation. The quartet of voltages that can impart these needed velocities is calculated using a pre-computed map that linearly relates the voltages to NW-velocities. See eqn (10) of our previous work[33] for a detailed theoretical derivation of the control law used in the present experiments. An output device applies this quartet of voltages at the electrodes, entraining the NW in fluid flow towards the target. Repeated executions of this feedback loop continually shape the fluid flow near the NW in a way that counteracts Brownian perturbations and enables the object to accurately track the desired trajectory. Specifically, translational flows move the wire and applied shear flows can rotate it. Although the shear flow shown in Fig. 1 is curl-free (irrotational), it will rotate the NW clockwise because the clockwise components of the flow will apply more torque on the long axis of the wire than the equal-and-opposite counter-clockwise components will apply on the short axis. Thus, the asymmetry of the wire allows it to be controllably rotated by an irrotational electro-osmotic flow.

We demonstrate the controlled translation and rotation of three electrically different objects - dielectric rods (made of SU8,[34] a photoresist), metallic (gold) NWs, and semiconducting (silicon) NWs - in water. Perturbations due to Brownian motion, residual pressure flows due to unequal heights of fluid in the device reservoirs, and possible non-uniformities in the zeta potential (potential differences across the Debye layer) at the device–fluid interface[35] are all compensated for by the feedback control loop.

The feedback loop in all experiments is updated in 33 ms time-steps (corresponding to the frame rate of the camera) with the magnitude of the maximum voltage at each of the electrodes limited to V_{max} = 10 V to prevent hydrolysis.[36]

Control of a 10 μm × 1 μm fluorescently labeled SU8 rod (lithographically fabricated in-house) in water is shown in movie M1 (see ESI,† movie is sped up to 4× real time), four snapshots of which are shown in Fig. 2. In each update of the feedback loop, the center of mass of the rod is directed towards a different target on the pre-planned path—the word "NIST" in Fig. 2—at an average speed of 4 μm s^{-1}. The rod is simultaneously rotated until its long axis is tangential to each segment in this path by the time its center of mass completes tracking that segment.[37]

The center of mass positional error along the x-axis at time-step i is defined as $e_{x,exp}(i) = x_{des}(i-1) - x_{obs}(i)$ where $x_{des}(i)$ and $x_{obs}(i)$ are the desired and observed x-coordinates of the rod center of mass at time step i. This definition respects the fact that the observed center of mass position at time-step i should be compared to the one demanded at time-step $i-1$. Mean $\langle e_{x,exp}(i)\rangle$ and root mean square (RMS) $\langle e^2_{x,exp}(i)\rangle^{1/2}$ values are measures of the x-positioning accuracy and precision respectively, averaged over the entire trajectory. The y-position error $e_{y,exp}(i) = y_{des}(i-1) - y_{obs}(i)$ and the orientational error $e_{\theta,exp}(i) = \theta_{des}(i-1) - \theta_{obs}(i)$ are defined similarly. Mean errors for this experiment were measured to be $\langle e_{x,exp}(i)\rangle = 0.22$ μm, $\langle e_{y,exp}(i)\rangle = 0.28$ μm and $\langle e_{\theta,exp}(i)\rangle = 1.3^\circ$. The RMS errors were $\langle e^2_{x,exp}(i)\rangle^{1/2} = 1.1$ μm, $\langle e^2_{y,exp}(i)\rangle^{1/2} = 1.2$ μm and $\langle e^2_{\theta,exp}(i)\rangle^{1/2} = 15.4^\circ$.

Next, the device performance was characterized by trapping individual SU8 rods (10 μm long, 1 μm wide, lithographically fabricated, in-house), silicon NWs (10 μm long, 100 nm wide, grown in-house) and gold NWs (10 μm long, 100 nm wide, methyl-terminated, Nanopartz Inc.[34]) at a fixed position and

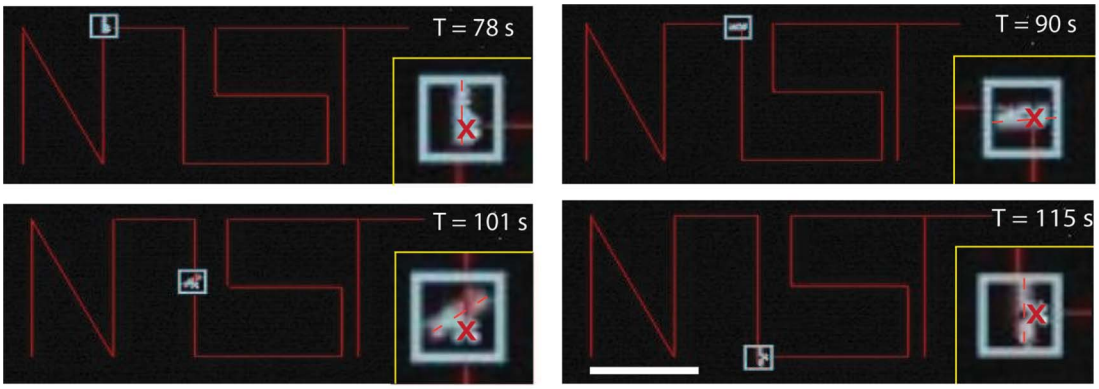

Fig. 2 Snapshots of a 10 μm × 1 μm fluorescently labeled SU8 rod being controlled along the ''NIST'' path graphically underlaid in red (movie M1 in ESI†). The rod is made to simultaneously rotate and align itself tangential to each of the 12 line segments by the time its center of mass reaches the end of a segment. Each image shows the rod at different locations along the trajectory at the noted times. The orientation of the rod is clarified in each inset with a dotted red line. The desired position of the rod's center of mass at the next time step is clarified in each inset with a red cross. Scale bar = 50 μm.

orientation. In each case, the NW was trapped positionally, rotated to an orientation of 0° and then maintained at that position and orientation for at least 45 s. Movies M2, M3 and M4 (see ESI,† all three movies in real time) show trapping of SU8, Si and Au NWs respectively. Fig. 3 shows snapshots and trajectories of the NWs while Table 1 lists errors.

Small and non-uniform optical scattering cross-sections of the Si and Au NWs occasionally results in NW image intensity falling below the camera noise threshold. Resultant errors in orientation estimates at such instants are recorded as spikes in the orientation time trace in Fig. 3. However, the control scheme is robust and control is resumed after the NW rotates past the spikes, as shown in the figure. Such errors could be reduced for critical applications by using a more sensitive camera and a darkfield objective.

Trapping errors scale with the relative strengths of the actuation and the diffusional perturbations. For a NW of length l, the rotational diffusion coefficient D_θ scales as l^{-3} whereas the translational diffusion coefficient scales as l^{-1}.[38] Simulations showed[33] that most of the voltage actuation is spent in compensating rotational, rather than translational, diffusion. Voltages required to completely compensate for the rotational diffusion perturbation frequently exceed the −10 V to 10 V range that was set to prevent hydrolysis. If the entirety of this range is available to combat rotational diffusion, then a Fokker–Planck analysis[39] yields (neglecting orientation measurement errors) the following theoretical RMS orientation error estimate for trapping

$$\langle e^2_{\theta,theo}\rangle^{1/2} = \sqrt{2}\frac{D_\theta}{\omega} \quad (1)$$

where ω is the angular velocity afforded by the voltage range that is available to combat rotational diffusion.

We now compare eqn (1) to experiments by independently measuring D_θ and ω for the three NWs that were trapped.

An additive diffusion noise model was used to estimate D_θ and the measurement noise $\sqrt{\langle\theta^2\rangle_{meas}}$, which arises due to camera noise and thresholding/pixelation errors in image processing (see ESI† and references 40,41 for details of this estimation). The diffusion coefficients for the SU8, Si and Au NWs were measured to be $(6 \pm 2) \times 10^{-3}$ rad^2 s^{-1}, $(4 \pm 1) \times 10^{-3}$ rad^2 s^{-1} and $(8 \pm 2) \times 10^{-3}$ rad^2 s^{-1} respectively while $\sqrt{\langle\theta^2\rangle_{meas}}$ measured 1.15°, 0.57° and 3.44° respectively.

The angular velocity ω that is available in experiments is lower than that suggested by the −10 V to 10 V voltage range. This is because part of the actuation is consumed in compensating for the residual pressure flow perturbation to NW motion that is observed in experiments (this perturbation is translatory in nature, see ESI†). The voltage range, and thus ω, that is effectively available for combating rotational diffusion is reduced as a result. The available ω is conservatively estimated to be the median of the angular velocities imparted by the actuation in each update of the feedback loop. The angular velocity imparted by EOFC in each update can be estimated by substituting the voltages, NW position and orientation values from each update into the EOF-physics based map relating the NW angular velocity to the applied voltages (see ESI†). The median angular velocity while trapping SU8, Si and Au NWs were measured to be 0.07 rad s^{-1}, 0.05 rad s^{-1} and 0.08 rad s^{-1} respectively. These values are substituted for ω in eqn (1), yielding theoretical estimates of RMS orientational precision that is comparable to the ≈5.4° precision observed experimentally (see Table 1). The lower values of the experimental precision compared to theoretical estimates in Table 1 suggests that the available angular velocity is in fact larger than the median used in the estimates.

Compared to other techniques for manipulating both the position and orientation of nano-objects, our main advantage is that we can manipulate NWs of any type (dielectric, semiconducting or metallic). Prior techniques for manipulating NWs have created potential wells, that counteract Brownian perturbations, by exploiting specific material properties of the NW, like its polarizability. For example, a 2 μm long SiNW was optically trapped in a recent experiment[11] to an oriental

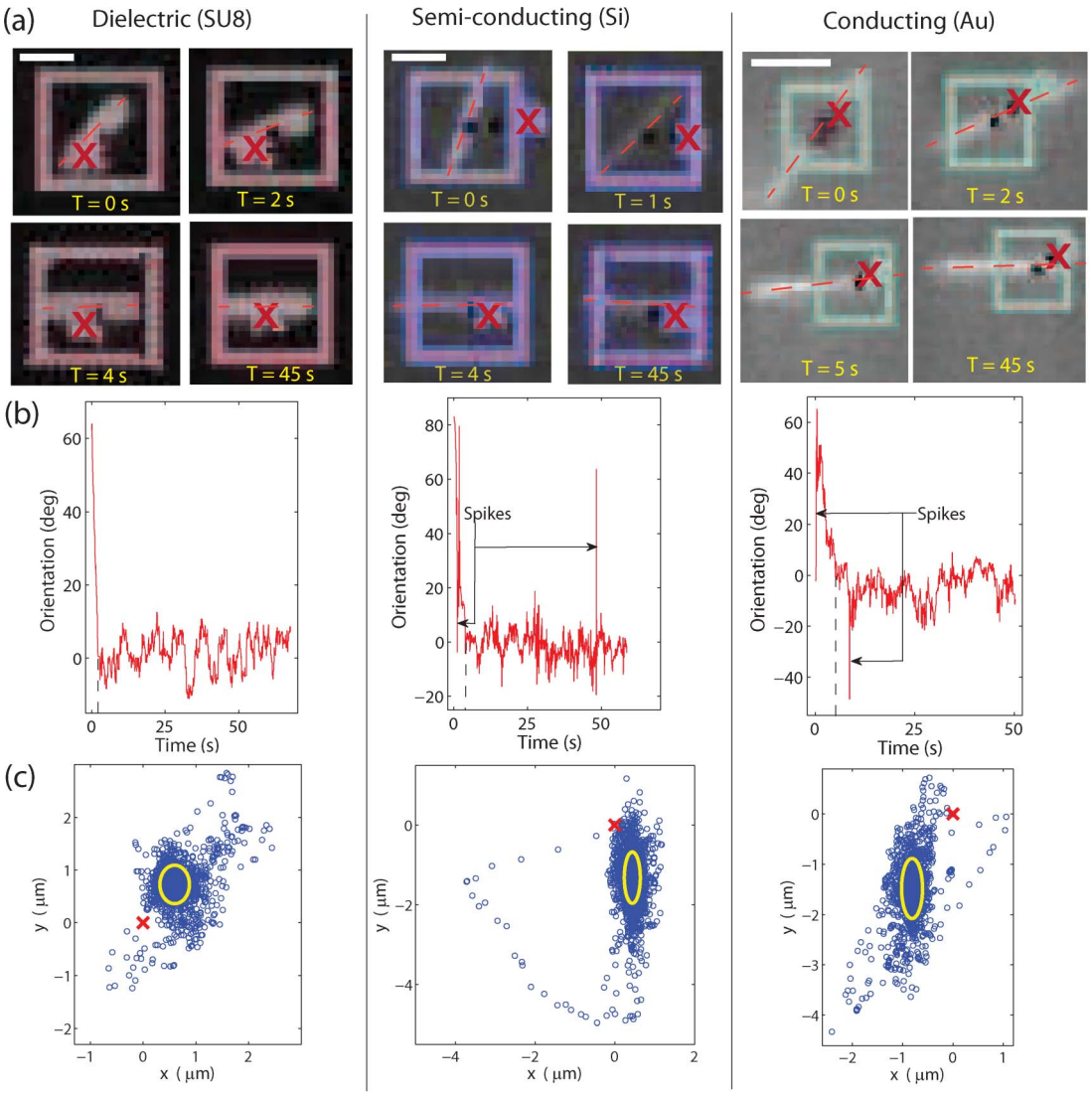

Fig. 3 Each of the three columns show rotation of a NW to $\theta = 0^\circ$ about a trapping location followed by holding at $\theta = 0^\circ$. Row (a) shows snapshots of NWs at indicated times with their orientations clarified by dotted red lines. Red crosses show the intended trapping position at (0,0). Scale bars = 5 μm. NW orientation data θ *versus* time t is shown in row (b). Spikes in $\theta(t)$ for Si and Au NWs indicate momentary errors in the orientation estimates due to NW image intensity falling below the camera's noise threshold but control is resumed after the NW rotates past the spikes. Black dotted lines indicate the time t_{FP} when the orientation of each NW first passes $\theta = 0^\circ$. Blue circles in row (c) plots show the NW center of mass estimates for times $t > 0$. Axes lengths of the yellow ellipse indicate RMS errors $\langle e^2_{x,exp}(i)\rangle^{1/2}$ and $\langle e^2_{y,exp}(i)\rangle^{1/2}$ for times $t(i) > t_{FP}$.

Table 1 Trapping errors for dielectric (SU8), semi-conducting (silicon) and conducting (gold) NWs: Each NW was trapped at a fixed position and orientation for at least 45 s. In the traps' absence, the expected RMS orientational deviation $\sqrt{\langle e^2_{\theta,exp}(i)\rangle}$ would exceed 40° within 45 s due to rotational diffusion. In the traps' presence, $\sqrt{\langle e^2_{\theta,exp}(i)\rangle}$ is lower than the theoretical estimate (last row) indicating that the available angular velocity is higher than the median used in the estimate

Error metric	SU8	SiNW	AuNW
$\langle e_{x,exp}(i)\rangle \pm \sqrt{\langle e^2_{x,exp}(i)\rangle}$	0.60 μm ± 0.28 μm	0.44 μm ± 0.20 μm	−0.81 μm ± 0.21 μm
$\langle e_{y,exp}(i)\rangle \pm \sqrt{\langle e^2_{y,exp}(i)\rangle}$	0.73 μm ± 0.37 μm	−1.31 μm ± 0.64 μm	−1.48 μm ± 0.60 μm
$\langle e_{\theta,exp}(i)\rangle \pm \sqrt{\langle e^2_{\theta,exp}(i)\rangle}$	1.52° ± 4.71°	−1.14° ± 5.33°	−4.28° ± 6.16°
$\sqrt{\langle e^2_{\theta,theo}\rangle} = \frac{180}{\pi}\cdot\frac{\sqrt{2}\langle D_\theta\rangle}{\omega}$	6.94°	6.48°	8.10°

precision of 3°. Micron sized silica and quartz particles have been rotated with angular velocities between 10 and 200 rad s^{-1}—a higher range than our technique—by exploiting properties like optical polarizability[10] and birefringence[16] (trapping precisions were not reported). For both optical and dielectrophoretic (DEP) actuations, trapping only works when the optical beam and AC electric fields respectively, are tuned to the dielectric properties of the NW.[13,25] Additionally, unlike our technique, high electric fields required for DEP necessitate electrode patterning near the control region (with such patterns however, parallel assembly of 15 μm long NWs, each spanning 10 μm × 1 μm sized inter-electrode gaps, has been shown[18]). In our technique, as long as the NW is bright enough to be imaged and thus spatially and orientationally localized, the feedback control technique does not depend on, nor is it significantly perturbed by, any other material properties of the NW.

3 Conclusion

We have experimentally demonstrated simultaneous position and orientation control of 10 μm long nanowires using electro-osmotic flow control (EOFC). Since fluid flow applies viscous forces to all material types, our method can be used to manipulate nanowires irrespective of which material they are made from - we demonstrate this by manipulating dielectric, semiconducting and metallic NWs. The wires are manipulated in a microfluidic device over a 170 μm × 170 μm control region with an average trapping precision of 0.6 μm in position and 5.4° in orientation. The flow control capability that we have shown here relies on fluid shear turning asymmetric objects, and will equally apply to manipulation of objects of other shapes. This technique can, in principle, be employed to map intensities and polarizations of microscale fields by scanning a probe object over the control region, material-independence would allow the selection of probes based on optimum sensitivity to the target field, without any constraint from the actuation mechanism.

Acknowledgements

We thank A. Berglund (CNST-NIST), R. Probst and Z. Cummins (both UMD) for helpful discussions. We also thank the following people at CNST-NIST: A. Band, D. Rutter and G. Holland for instrument setup; A. Talin and D. Ruzmetov for providing a sample of SiNWs. PPM acknowledges support under the cooperative research agreement between UMD and NIST-CNST (award 70NANB10H193).

References

1 Y. Fang, Z. Li, Y. Huang, S. Zhang, P. Nordlander, N. J. Halas and H. Xu, Branched Silver Nanowires as Controllable Plasmon Routers, *Nano Lett.*, 2010, **10**(5), 1950–1954.
2 D. J. Sirbuly, M. Law, P. Pauzauskie, H. Yan, A. V. Maslov, K. Knutsen, C-Z. Ning, R. S. Saykally and P. Yang, Optical Routing and Sensing with Nanowire Assemblies, *Proc. Natl. Acad. Sci. U. S. A.*, 2005, **102**(22), 7800–7805.
3 Y. Nakayama, P. J. Pauzauskie, A. Radenovic, R. M. Onorato, R. J. Saykally, J. Liphardt and P. Yang, Tunable Nanowire Nonlinear Optical Probe, *Nature*, 2007, **447**, 1098–1102.
4 D. Fan, Z. Yin, R. Cheong, F. Q. Zhu, R. C. Cammarata, C. L. Chien and A. Levchenko, Subcellular-resolution Delivery of a Cytokine through Precisely Manipulated Nanowires, *Nat. Nanotechnol.*, 2010, **5**, 545–551.
5 F. Favier, E. C. Walter, M. P. Zach, T. Benter and R. M. Penner, Hydrogen Sensors and Switches from Electrodeposited Palladium Mesowire Arrays, *Science*, 2001, **293**, 2227–2231.
6 C. Ropp, R. Probst, Z. Cummins, R. Kumar, A. Berglund, S. R. Raghavan, E. Waks and B. Shapiro, Manipulating Quantum Dots to Nanometer Precision by Control of Flow, *Nano Lett.*, 2010, **10**(7), 2525–2530.
7 V. Bingelyte, J. Leach, J. Courtial and M. J. Padgett, Optically controlled three-dimensional rotation of microscopic objects, *Appl. Phys. Lett.*, 2003, **82**(5), 829–831.
8 A. T. O Neil and M. J. Padgett, Rotational control within optical tweezers by use of a rotating aperture, *Opt. Lett.*, 2002, **27**(9), 743–745.
9 R. Dasgupta, P. K. Mohanty and P. K. Gupta, Controlled Rotation of biological microscopic objects using optical line tweezers, *Biotechnol. Lett.*, 2003, **25**, 1625–1628.
10 L. Paterson, M. P. MacDonald, J. Arlt, W. Sibbett, P. E. Bryant and K. Dholakia, Controlled Rotation of Optically Trapped Microscopic Particles, *Science*, 2001, **292**, 912–914.
11 A. Irrera, P. Artoni, R. Saija, P. Gucciardi, M. Iati, F. Borghese, P. Denti, F. Iacona, F. Priolo and O. Marago, Size Scaling in Optical Trapping of Silicon Nanowires, *Nano Lett.*, 2011, **11**, 4879–4884.
12 K. C. Neuman, E. H. Chadd, G. F. Liou, K. Bergman and S. M. Block, Characterization of Photodamage to *Escherichia coli* in Optical Traps, *Biophys. J.*, 1999, **77**(5), 2856–2863.
13 P. J. Pauzauskie, A. Radenovic, E. Trepagnier, H. Shroff, P. Yang and J. Liphardt, Optical trappng and integration of semiconductor NW assemblies in water, *Nat. Mater.*, 2006, **5**, 97–101.
14 P. V. Ruijgrok, N. R. Verhart, P. Zijlstra, A. L. Tchebotareva and M. Orrit, Brownian Fluctuations and Heating of an Optically Aligned Gold Nanorod, *Phys. Rev. Lett.*, 2011, **107**, 1–4.
15 M. E. J. Friese, T. A. Nieminen, N. R. Heckenberg and H. Rubinsztein-Dunlop, Optical alignment and spinning of laser-trapped microscopic particles, *Nature*, 1998, **394**, 348–350.
16 A. La Porta and M. D. Wang, Optical Torque Wrench: Angular Trapping, Rotation, and Torque Detection of Quartz Microparticles, *Phys. Rev. Lett.*, 2004, **92**, 190801.
17 B. Edwards, N. Engheta and S. Evoy, Electric tweezers: Experimental study of positive dielectrophoresis-based positioning and orientation of a nanorod, *J. Appl. Phys.*, 2007, **102**, 024913.

18 S. Raychaudhuri, S. A. Dayeh, D. Wang and E. T. Yu, Precise Semiconductor Nanowire Placement Through Dielectrophoresis, *Nano Lett.*, 2009, **9**(6), 2260–2266.

19 K. D. Hermanson, S. O. Lumsdon, J. P. Williams, E. W. Kaler and O. D. Velev, Dielectrophoretically assisted assembly of electrically functional microwires from nanoparticle suspensions, *Science*, 2001, **294**, 1082–1086.

20 P. A. Smith, C. D. Nordquist, T. N. Jackson and T. S. Mayer, Electric-field assisted assembly and alignment of metallic nanowires, *Appl. Phys. Lett.*, 2000, **77**(9), 1399–1401.

21 A. Jamshidi, P. J. Pauzauskie, P. J. Schuck, A. T. Ohta, P. Chiou, J. Chou, P. Yang and M. C. Wu, Dynamic manipulation and separation of individual semiconducting and metallic nanowires, *Nat. Photonics*, 2008, **2**, 85–89.

22 W. Ahmed, E. S. Kooij, A. van Silfhout and B. Poelsema, Quantitative Analysis of Gold Nanorod Alignment after Electric Field-Assisted Deposition, *Nano Lett.*, 2009, **9**(11), 3786–3794.

23 L. Altomare, M. Borgatti, G. Medoro, N. Manaresi, M. Tartagni, R. Guerrieri and R. Gambari, Levitation and Movement of Human Tumor Cells Using a Printed Circuit Board Device based on Software-controlled Dielectrophoresis, *Biotechnol. Bioeng.*, 2003, **82**(4), 474–479.

24 C. H. Lee, D. R. Kim and X. Zheng, Orientation Controlled Alignment of Axially Modulated on Silicon Nanowires, *Nano Lett.*, 2010, **10**, 5116–5122.

25 E. M. Freer, O. Grachev and D. P. Stumbo, High yield self limiting single nanowire assembly with dielectrophoresis, *Nat. Nanotechnol.*, 2010, **5**, 525–530.

26 L. Zhang, J. J. Abbott, L. Dong, B. E. Kratochvil, D. Bell and B. J. Nelson, Artificial bacterial flagella: Fabrication and magnetic control, *Appl. Phys. Lett.*, 2009, **94**, 064107.

27 L. Sacconi, G. Romano, R. Ballerini, M. Capitanio, M. De Pas and M. Giuntini, Three-dimensional magneto-optic trap for micro-object manipulation, *Opt. Lett.*, 2001, **26**(17), 1359–1362.

28 L. Zhang, J. J. Abbott, L. Dong, K. E. Peyer, B. E. Kratochvil, H. Zhang, C. Bergeles and B. J. Nelson, Characterizing the Swimming Properties of Artificial Bacterial Flagella, *Nano Lett.*, 2009, **9**(10), 3663–3667.

29 D. H. Reich, M. Tanase, A. Hultgren, L. A. Bauer, C. S. Chen and G. J. Meyer, Biological Applications of multifunctional magnetic nanowires, *J. Appl. Phys.*, 2003, **93**(10), 7275–7280.

30 T. Petit, L. Zhang, K. E. Peyer, B. E. Kratochvil and B. J. Nelson, Selective Trapping and Manipulation of Microscale Objects Using Mobile Microvortices, *Nano Lett.*, 2012, **12**(1), 156–160.

31 R. F. Probstein, *Physicochemical Hydrodynamics*, New York, Wiley, 1994.

32 It takes less than Tss = 1 ms, from application of an electric field, for a fluid to achieve steady state velocity in a 10 μm thick channel. See derivation for T_{ss} in N. A. Patankar and H. H. Hu, Numerical simulation of electro-osmotic flow, *Anal. Chem.*, 1998, **70**(9), 1870–1881.

33 P. P. Mathai, A. J. Berglund, J. A. Liddle and B. Shapiro, Simultaneous Positioning and Orientation of a Single Nano-object by Flow Control: Theory and Simulations, *New J. Phys.*, 2011, **13**, 013027.

34 All referencesto commercial products in this paper are provided only to document how results have been obtained. Their identification does not imply recommendation or endorsement by NIST.

35 H. T. Baytekin, A. Z. Patashinski, M. Branicki, B. Baytekin, S. Soh and B. A. Grzybowski, The Mosaic of Surface Charge in Contact Electrification, *Science*, 2011, **333**(6040), 308–312.

36 If the maximum $V_{\max}^{\text{des}}$ among the magnitudes of the computed voltage quartet $V^{des}(i)$, i = 1,...,4 desired by the controller exceeds V_{max}, then the voltages that are applied at the electrodes during the control update are the linearly scaled $V^{app}(i) = \frac{V_{max}}{V_{max}^{des}} V^{des}(i), i = 1,..,4$. This scaling limits the magnitude of the maximum translational and rotational velocity that can be imparted to the object in an update but does not change the direction of those velocities.

37 There are 12 line segments in the ''NIST'' path (including the penultimate segment where it partially retraces the segment preceding it). Along the first segment, the desired orientation of the rod is maintained at $\theta = 90^\circ$ where θ is the angle between the long axis of the rod and the scale bar in Fig. 2. For segments k = 2 to k = 12, if the rod has been translated along that segment by a fraction f of the length of that segment, then its desired orientation at that point is $\theta_{des}(f) = f\theta_k + (1 - f)\theta_{k-1}$ where θ_k is the orientation of segment k.

38 H. Brenner, The Stokes resistance of an arbitrary particle - Part IV. Arbitrary fields of flow, *Chem. Eng. Sci.*, 1964, **19**, 703–727.

39 The simplified rotational dynamics for a nanowire trapped by EOFC is given by the stochastic differential equation $d\theta = -\omega \cdot \text{sign}(\theta) dt + (2D_\theta dt)^{1/2} \mathcal{N}(0,1)$ where $\mathcal{N}(0,1)$ is the unit normal random variable. For an ideal ellipsoidal rod, with minor to major axis length ratio α, we have $\omega = \frac{1-\alpha^2}{1+\alpha^2} \sigma_{max}$ where σ_{max} is the maximum shear velocity that can be electro-osmotically imparted to the fluid. See ref. 33 for details.

40 K. A. Rose, J. A. Meier, G. M. Dougherty and J. G. Santiago, Rotational Electrophoresis of Striped Metallic Microrods, *Phys. Rev. E: Stat., Nonlinear, Soft Matter Phys.*, 2007, **75**, 1–15.

41 J. C. Crocker and D. G. Grier, Methods of Digital Video Microscopy for Colloidal Studies, *J. Colloid Interface Sci.*, 1996, **179**, 298–310.

Supplementary Information

1 Electro-osmotic flow

Electro-osmotic flow is proportional to the applied electric field.[1] As shown in the cross-sectional view in Fig. 1, the applied field moves the counter-ions in the Debye layer at the interface of the device and the fluid (in our experiments, the fluid is water). The motion of the counter-ions moves the rest of the fluid due to viscous drag with the flow velocity being directly proportional to the applied electric field.

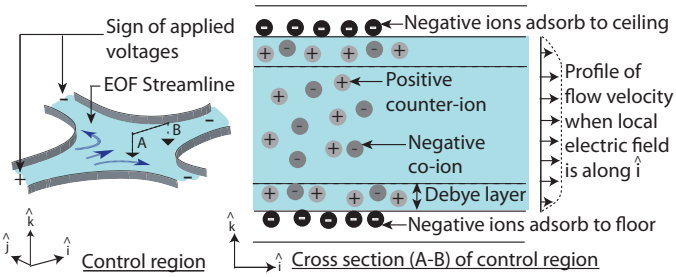

Fig. 1 The left panel shows the streamlines of the flow following the applied electric field. The flow profile in the device (along section A-B of the left panel) is shown in the right panel.[1] The naturally occurring negatively charged ions adsorbed to the surface of the device are shielded by positively charged ions from the fluid. The ions in the thin diffuse (Debye) layer near the device-fluid interface move under the influence of the electric field and drag the rest of the fluid by viscous forces.[1] The resulting electro-osmotic flow profile is uniform along $\hat{k}$ (except for the variation in the thin Debye layer, not drawn to scale) with the flow velocity proportional to the applied electric field. Objects like NWs that are suspended in the fluid are entrained in this flow.

Spatio-temporal variations of the applied electric field pattern moves the carpet of counter-ions, and consequently the fluid, along that pattern, translating an immersed object over any desired path in the same way that moving a carpet in a room results in the movement of furniture placed on it. EOF is irrotational (staying with the analogy, rotating the carpet is disallowed) because the underlying electric field is curl-free. An immersed object needs to be less symmetric than a sphere (for example, rod-shaped) for EOF shear to be able to rotate it.[2,3]

2 Estimating the center of mass and orientation of NW

The center of mass (x_{cm}, y_{cm}) of the NW in every feedback update was found by thresholding on the pixel brightness. In every update a square window, 45 pixels on a side, centered around the previous center of mass estimate was considered for image processing (this window was found to be large enough to accommodate the largest possible translation of the NW in the previous update). Every contiguous set of sufficiently bright pixels in this window was considered as a possible contender of the NW image, with a pixel declared as sufficiently bright if it was at least 40% as bright as the brightest pixel in the window. The center of mass of each of these contenders was computed, with the true NW center of mass (x_{cm}, y_{cm}) declared as the one which was closest to the center of mass estimate in the previous feedback update. The set S_{NW} of sufficiently bright contiguous pixels, with coordinates (x_i, y_i), having center of mass (x_{cm}, y_{cm}) was declared as the current image of the NW.

The orientation θ of the NW, defined to lie in the range $R_{\frac{\pi}{2}} = (\frac{-\pi}{2}, \frac{\pi}{2}]$, was then estimated as the orientation of the line passing through (x_{cm}, y_{cm}) that was a least-squares best fit to the pixels in the set S_{NW} that comprised the NW image. The orientation θ of the NW should then, due to the fit, satisfy

$$\tan(2\theta) = \frac{2\langle x_i y_i \rangle}{\langle y_i^2 \rangle - \langle x_i^2 \rangle} \quad (1)$$

where (x_i, y_i) are the pixel co-ordinates measured with respect to the origin (x_{cm}, y_{cm}) and $\langle . \rangle$ denotes the averaging operator. Thus the orientation θ of the NW can be obtained by using Eqn. 1 with two caveats:
(1) If $\langle y_i^2 \rangle = \langle x_i^2 \rangle$ then $\theta = \pm\frac{\pi}{4}$. This ambiguity was resolved by declaring $\theta = \frac{\pi}{4}$ if $\langle x_i y_i \rangle > 0$ and $\theta = -\frac{\pi}{4}$ otherwise.
(2) Even if $\langle y_i^2 \rangle \neq \langle x_i^2 \rangle$, Eqn. 1 gives two possible choices for θ since $\tan(2\theta) = \tan(2\theta - \pi)$. In this case, exactly one of these choices lies in the range $R_{\frac{\pi}{4}} = (\frac{-\pi}{4}, \frac{\pi}{4})$. The NW orientation was declared to lie in $R_{\frac{\pi}{4}}$ if $\langle x_i^2 \rangle > \langle y_i^2 \rangle$ and in $(R_{\frac{\pi}{2}} - R_{\frac{\pi}{4}})$ if $\langle x_i^2 \rangle < \langle y_i^2 \rangle$.

3 Measurement of median angular velocity and rotational diffusion coefficient

We first describe the measurement of the median NW angular velocity imparted by electro-osmotic flow control (EOFC) during the trapping phase of the experiment (when the NW is held at a fixed position and orientation) for the three (SU8, Si and Au) NWS. We then describe the measurement of the rotational diffusion coefficient D_θ for the three NWs.

For measuring the median angular velocity, we first estimated a list $\{\omega(i)\}$ of EOFC-imparted NW angular velocities during each feedback update i of the trapping phase. For each i we substitute the applied experimental voltages, and the measured NW position and orientation values in an EOF-physics based map relating the NW angular velocity to the applied

voltages (see Eqn. 7 of previous work[3]) to get $\{\omega(i)\}$. The zeta potential magnitude at the device-fluid interface used in this estimate was[4] 50 mV, viscosity of water was[5] 8.9×10^{-4} Pa.s and relative dielectric permittivity of water was[5] 80. For each NW, the median of $\{\omega(i)\}$ is estimated to be the angular velocity ω that is available to combat rotational diffusion.

We measured D_θ for each of the three same objects that were trapped by measuring their mean square rotational displacements when they were each allowed to freely move after the trapping experiments. Each object was tracked until it drifted to the edge of the control region. In the manner described in Rose et al.,[6] the orientation of the objects were fit using linear regression to the additive diffusion/noise model $\langle\theta^2_{exp}\rangle = 2D_\theta t + \langle\theta^2_{meas}\rangle$, where $\langle\theta^2_{exp}\rangle$ is the mean squared deviation of the experimentally measured rotation and $\langle\theta^2_{meas}\rangle$ is the mean squared measurement noise (the justification for such an additive noise model for diffusional motion of colloids is detailed in Crocker et al.[7]). This was repeated at least three times per object (once it reached the edge of the control region, the NW was brought back towards the center of the center of the control region (by EOF) and allowed to freely move once again). The rotational diffusion coefficients, fitted to the additive diffusion model, and averaged over the multiple experiments were measured to be $6\pm2\times10^{-3}$ rad^2/s for the SU8 rod, $4\pm1\times10^{-3}$ rad^2/s for the SiNW and $8\pm2\times10^{-3}$ rad^2/s for the AuNW. The measurement noises were measured to be 0.02 rad, 0.01 rad and 0.06 rad respectively.

4 Motion due to residual pressure flow

The fluid in the reservoirs of our device experience an unbalanced surface tension that creates a background residual pressure flow that perturbs NW motion. This perturbation, compensated by EOFC, becomes evident when control is switched off as is the case while measuring D_θ.

The perturbation has a significant translatory effect on the NW motion as can be seen by the almost linear graph of the translational displacement in Fig. 2 (a stochastic translational diffusion component negligibly adds to the linear component). The strength of the NW translation due to residual pressure flow can be compared to that of Brownian translation by comparing transit times in the control region. As seen in Fig. 2, the SU8 rod was transported by a distance of 75 μm to the edge of the control region within $\approx$ 30 s due to the residual pressure flow (so v_{press}, the translational velocity due to residual pressure flow, is less than 3 μm/s - we use v_{press} to estimate the effect of induced charge electrophoresis in the next section). Without the residual pressure flow, translational diffusion by itself would have required $>$ 9000 s to move the rod by the same distance.[8]

However, as shown in Fig. 2, the stochastic nature of the *rotational* Brownian motion is *not* affected by the residual pressure flow. For comparison, a 10 μm $\times$1 μm cylindrical rod in water at room temperature, far from the device walls, has a theoretical rotational diffusion coefficient of 8.4×10^{-3} rad^2/s.[9] The proximity of the rod to the floor of the device is responsible[10] for the ($\approx$ 25%) lower experimental values mentioned above. The lower values show that the residual pressure flow does not significantly add to the rotational mean squared deviations used to estimate D_θ.

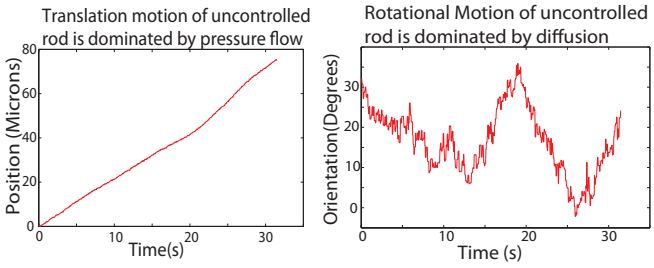

Fig. 2 Rotational displacements of an uncontrolled SU8 rod is dominated by rotational diffusion but its translation is dominated by residual pressure flow.

5 Other forces affecting NW motion

Induced charge electrophoresis (ICEP) due to the applied electric field can have a perturbatory effect on NW motion. ICEP affects rotational,[13] but not translational, motion of nanowires in an electric field. We compare the angular velocities due to ICEP and EOF in the following. The angular velocity ω_{ICEP} due to ICEP, can be bounded by $\omega_{ICEP} \leq \frac{\varepsilon E^2}{6\mu}$ (see SI of our previous work[3]) where μ and ε are the viscosity (8.9×10^{-4} Pa.s) and relative dielectric permittivity (80) of water[5] respectively and E is the magnitude of the local electric field strength. The local electric field strength in our device is spent on countering translation, while the electric field gradient is spent on countering rotation. Since the translation being countered is mostly due to residual pressure flow, the magnitude of the electric field strength needed to counter it using EOF is $E = \frac{v_{press}\mu}{\varepsilon\zeta}$, where the magnitude of the zeta potential at the device-fluid interface is[4] $\zeta = 50$ mV and v_{press} is the translational velocity due to residual pressure flow that is being countered by EOF. Since $v_{press} < 5$ μm/s in our experiments, we get after substituting values, $\omega_{ICEP} \leq 2\times10^{-3}$ rad/s. This is less than 3.5 % of the median rotational velocity of the NWs observed in our experiments. Thus we conclude that ICEP negligibly affects NW rotational velocity in our device.

References

1 R.F. Probstein, *Physicochemical Hydrodynamics*, New York, Wiley, 1994.

2 H. Brenner, "The Stokes resistance of an arbitrary particle - Part IV. Arbitrary fields of flow" *Chemical Engineering Science*, 19, pp. 703-727, 1964.

3 P. P. Mathai, A. J. Berglund, J. A. Liddle and B. Shapiro, "Simultaneous Positioning and Orientation of a Single Nano-object by Flow Control: Theory and Simulations," *New Journal of Physics*, 13, 013027, 2011.

4 M. D. Armani, S. V. Chaudhary, R. Probst, and B. Shapiro, "Using feedback control of microflows to independently steer multiple particles," *Journal of Microelectromechanical Systems*, 15, 4, pp. 945-954, August 2006.

5 D. R. Lide (Editor-in-chief) *CRC handbook of Chemistry and Physics*, CRC press, Ed. 90, 2009.

6 K. A. Rose, J. A. Meier, G. M. Dougherty, J. G. Santiago, "Rotational Electrophoresis of Striped Metallic Microrods," *Physical Review E*, 75, 011503:1-15, 2007.

7 J. C. Crocker and D. G. Grier, "Methods of Digital Video Microscopy for Colloidal Studies," *Journal of Colloid Interface Science*, 179, pp.298-310, 1996.

8 The translational diffusion coefficients perpendicular and parallel to the long axis of a cylindrical rod[11] are $D_\perp = \frac{kT\cdot(log(2l/d)+0.5)}{4\pi\eta l} = 0.13\ \mu\text{m}^2/\text{s}$ and $D_\parallel = \frac{kT\cdot(log(2l/d)-0.5)}{2\pi\eta l} = 0.18\ \mu\text{m}^2/\text{s}$ respectively for the SU8 rod immersed in water at room temperature, where l is the length of the rod, d is the diameter, k is the Boltzmann constant, T is the temperature, η is the dynamic viscosity of water. A root mean squared displacement of 75 μm due to translational diffusion alone would thus require 9072 s on average.

9 $D_\theta = \frac{3kT}{\pi\eta l^3}(log(l/d) + log(4) - 11/16)$ where l is the length of the rod, d is the diameter, k is the Boltzmann constant, T is the temperature, η is the dynamic viscosity of water. See derivation in: H. Yamakawa, "Viscoeleastic Properties of Straight Cylindrical Macromolecules in Dilute Solution," *Macromolecules*, 8, 3, pp.339-342, 1975.

10 J. T. Padding and W. J. Briels, "Translational and rotational friction on a colloidal rod near a wall," *The Journal of Chemical Physics*, 132, pp. 054511-1:8, 2010.

11 J. Happel and H. Brenner, *Low Reynolds Number Hydrodynamics*, Englewood Cliffs, Prentice Hall, 1965.

12 A. Sellier, "A note on the electrophoresis of a uniformly charged particle," *Quarterly Journal of Mathematics and Applied Mechanics*, 55, 4, pp.561-572, 2002.

13 D. Saintillan, E. Darve, and E. S. G. Shaqfeh, "Hydrodynamic Interactions in the induced-charge electrophoresis of colloidal rod suspensions," *Journal of Fluid Mechanics*, 563, pp.223-259, 2006.